

# Multiple Emission of Phosphonium Fluorophores Harnessed by the Pathways of Photoinduced Counterion Migration

Andrey Belyaev,\* Bo-Kang Su, Yu-Hsuan Cheng, Zong-Ying Liu, Nasrulla Majid Khan, Antti J. Karttunen,\* Pi-Tai Chou,\* and Igor O. Koshevoy\*

**Abstract:** In the emerging field of intramolecular charge transfer induced counterion migration, we report the new insights into photophysical features of luminescent donor–acceptor phosphonium dyes ( $D-\pi-\pi_n A^+[X^-]$  ( $\pi = -(C_6H_4)_x-$ ). The unique connectivity of the phosphorus atom affords multipolar molecules with a variable number of arms and the electronic properties of the acceptor group. In the ion-paired form, the transition from dipolar to quadrupolar configuration enhances the low energy migration-induced band by providing the additional pathways for anion motion. The multipolar architecture, adjustable lengths of the  $\pi$ -spacers and the nature of counterions allow for efficient tuning of the emission and achieving nearly pure white light with quantum yields around 30%. The methyl substituent at the phosphorus atom reduces the rate of ion migration and suppresses the red shifted bands, simultaneously improving total emission intensity. The results unveil the harnessing of the multiple emission of phosphonium fluorophores by anion migration via structure and branching of donor–acceptor arms.

## Introduction

Light-driven molecular motion is a fascinating property, which forms a basis for the development of unconventional materials,<sup>[1]</sup> molecular switches, motors and machines.<sup>[2]</sup> A major strategy to photo-controlled movement of molecular components relies on the use of isomerizable organic units that ensures robustness of such photodynamic systems and simultaneously defines their functional behavior.<sup>[3]</sup> Alternatively, the change of the electronic structure that occurs upon photoexcitation can perturb non-covalent contacts between the constituents of supramolecular species and affect their mutual displacement.<sup>[4]</sup> Thus, switching hydrogen-bonding ability or electrostatic interactions by means of photoinduced electron transfer allowed one to realize fast (ca. 1–100  $\mu$ s) translational motion in a rotaxane type of molecular shuttles.<sup>[5]</sup> The employment of a photoacidic moiety capable of intermolecular proton transfer in a rotaxane structure allowed one to increase the rate of translocation on a distance of ca. 1 nm nearly by an order of magnitude.<sup>[6]</sup> Even faster movement occurring on a pico-second time scale driven by excited-state intramolecular charge transfer (ESICT) has been proposed for pyridinium donor–acceptor dyes embedded in the cucurbit[7]uril host.<sup>[7]</sup> However, the relocations of the composite elements in these photo-driven (pseudo)rotaxane shuttles typically generate very limited alterations of optical characteristics, which hardly can serve as convenient read-out signals.

The sensitivity of CT state of organic chromophores to the polarity of the local environment nevertheless potentially offers an attractive opportunity to design molecular systems, demonstrating motion-produced optical function at high speed and in a reversible manner. For instance, it has been shown that photoexcitation of a donor–acceptor (D–A) dye combined with a calixarene receptor leads to very fast translocation of a coordinated potassium ion within the host molecule, which is clearly reflected in time-resolved absorption spectra.<sup>[8]</sup> In the case of ionic  $D-\pi-A^+$  fluorophores, the CT-modulated interactions within non-dissociated ion pairs have been noticed to exhibit a more pronounced photophysical response.<sup>[9]</sup> Recently, we reported structurally simple linear  $D-\pi-A^+$  fluorophores with phosphonium and pyridinium acceptor  $A^+$  units ( $D = -NR_2$  group,  $\pi =$  phenylene spacer),<sup>[10]</sup> which reveal regular photoinduced CT and depletion of electron density from the donor motif. The redistribution of electron density and the formation of the  $-N^{\delta+}R_2$  site<sup>[8]</sup> is stabilized in polar solvents by dipole–dipole interactions with a rapidly reorganized nearest shell of the

[\*] Dr. A. Belyaev, N. M. Khan, Prof. I. O. Koshevoy  
 Department of Chemistry  
 University of Eastern Finland  
 Yliopistokatu 7, 80101 Joensuu (Finland)  
 E-mail: andrei.beljaev@tu-dortmund.de  
 igor.koshevoy@uef.fi

B.-K. Su, Y.-H. Cheng, Z.-Y. Liu, Prof. P.-T. Chou  
 Department of Chemistry  
 National Taiwan University  
 Taipei 106 (Taiwan)  
 E-mail: chop@ntu.edu.tw

Prof. A. J. Karttunen  
 Department of Chemistry and Materials Science  
 Aalto-University  
 00076 Aalto (Finland)  
 E-mail: antti.j.karttunen@iki.fi

© 2022 The Authors. Angewandte Chemie International Edition published by Wiley-VCH GmbH. This is an open access article under the terms of the Creative Commons Attribution License, which permits use, distribution and reproduction in any medium, provided the original work is properly cited.

medium. On the contrary, in solvents with low polarity, the photophysical behavior of these dyes is strongly influenced by the ion-pairing effect. The latter is manifested by ESICT-driven migration (or translocation) of a small counter anion from the cationic  $A^+$  area (ground state location) in the direction of the transient  $-N^{\delta+}R_2$  group (excited state target) that decreases the energy of the emissive state and leads to the evolution of a continuum of red-shifted fluorescence bands (Scheme 1). The resulting dual-band-like steady-state luminescence was shown to be dependent on the length of the  $\pi$ -spacer, the size of migrating anion, and the solvent viscosity. Comparison of phosphonium<sup>[10a]</sup> and pyridinium<sup>[10b]</sup> congeners also indicate the important role of the cationic group and, consequently, polarization of the spacer in the process of light-triggered anion migration and corresponding optical response.

In this emerging field, herein, we aim at exploring the factors affecting the ESICT-induced ion motion and photophysical features of emissive ion-paired  $D-\pi-A^+$  salts ( $\pi = -(C_6H_4)_x-$ ) via a new series of phosphonium dyes with various branching CT chromophores. The strategy lies in the unique connectivity and accessible quaternization of the phosphorus atom,<sup>[11]</sup> which allow us to synthesize novel multipolar molecules  $(D-\pi-)_nA^+$  with variable number of and length of linear donor-acceptor arms,  $^+PPh_{4-n}(-\pi-D)_n$  ( $n=1-4$ ) and  $^+PPh_2(-\pi-D)(-\pi'-D)$ . To probe the cationic effect, we also chemically alter the acceptor group by introducing the methyl group along the aromatic substituents in  $^+PMePh_{3-m}(-\pi-D)_m$  ( $m=1, 3$ ). The results elaborated below, for the first time, unveil the key role played by cation structure and donor-acceptor arms to the ESICT-driven counterion migration and hence to the harnessing of the multiple emission.

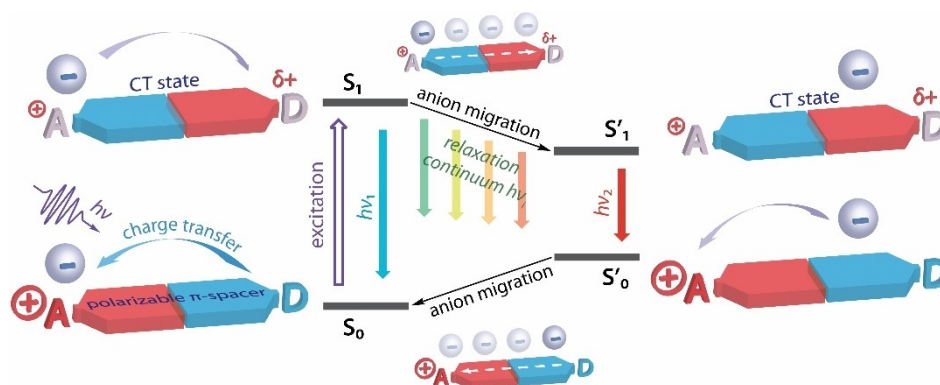
## Results and Discussion

### Synthesis and Characterization

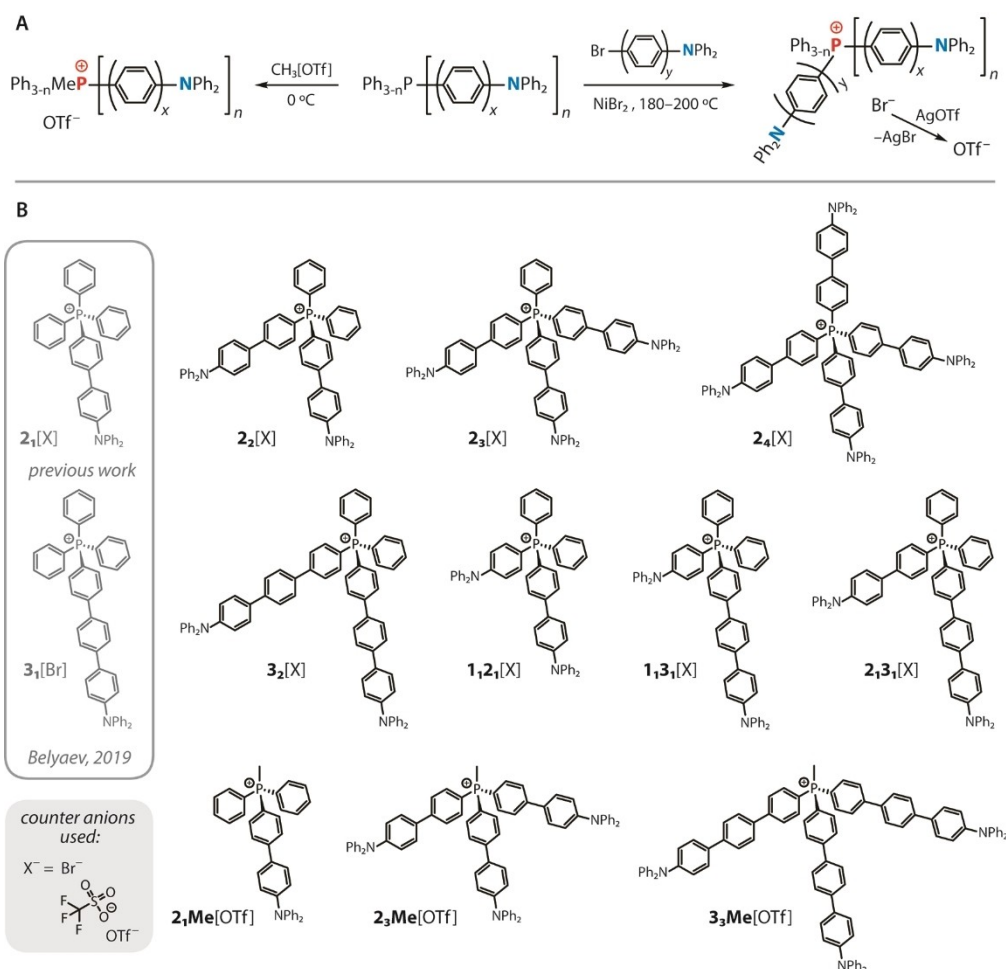
The preparation of  $(D-\pi-)_nA^+[X^-]$  phosphonium dyes is outlined in Scheme 2, where the experimental details are given in the Supporting Information. Following the general

NiBr<sub>2</sub>-catalyzed protocol,<sup>[12]</sup> the reactions of appropriate donor-functionalized phosphines  $PPh_{3-n}[-(C_6H_4)_x-NPh_2]_n$  ( $x=2, n=1$  **L2**<sub>1</sub>,<sup>[13]</sup> **3 L2**<sub>3</sub>;<sup>[14]</sup>  $x=3, n=1$  **L3**<sub>1</sub>, **3 L3**<sub>3</sub><sup>[14]</sup>) with the corresponding bromo-*N,N*-diphenyl-aryl amines, Br- $(C_6H_4)_y-NPh_2$  ( $y=1-3$ ),<sup>[15]</sup> or bromobenzene (for **2**<sub>3</sub>[Br]) afford tetraaryl bromide salts, which were isolated as amorphous solids. These quaternized cationic species are designated as  $Y_nZ_{n'}[Br]$ , where *Y* and *Z* correspond to the length of phenylene linkers and the *n*, *n'* subscripts indicate the number of the respective donor-containing substituents. Compounds **2**<sub>2</sub>[Br] and **2**<sub>3</sub>[Br] are obtained in good yields (77 and 80%), and for the rest of the series the target compounds are generated with visibly smaller efficiency (34–52%). The Pd-catalyzed formation of phosphonium ions<sup>[16]</sup> in this case is found to be less selective; for instance, the reactions of equimolar amounts of **L2**<sub>1</sub> and Br- $(C_6H_4)_y-NPh_2$  give mixtures of several P-cationic products (Figure S1), which are difficult to separate. Whereas selectivity of the process can be significantly improved by lowering the temperature from 140 to ca. 115 °C, the overall conversion of the starting materials does not exceed 30%. A phenol-promoted metal-free approach<sup>[17]</sup> also delivers moderate to low yields (13% for **2**<sub>2</sub>[Br] and 10% for **2**<sub>3</sub>[Br]) because of limited solubility of the oligophenylene phosphine precursors **L2**<sub>1</sub> and **L2**<sub>3</sub>. Salts **2**<sub>1</sub>[X] and **3**<sub>1</sub>[Br] have been studied by us previously.<sup>[10a]</sup> The metathesis of the counterion  $Br^- \rightarrow OTf^-$  was performed with silver(I) triflate in a nearly quantitative manner. Methylation of phosphines **L2**<sub>1</sub>, **L2**<sub>3</sub> and **L3**<sub>3</sub> was readily carried out with methyl triflate, giving salts **2**<sub>1</sub>Me[OTf], **2**<sub>3</sub>Me[OTf] and **3**<sub>3</sub>Me[OTf] in 83–93% yield.

The composition of the products was confirmed by spectroscopic methods. The ESI<sup>+</sup> mass spectra of all salts show one dominating signal that in each case corresponds to the molecular cation (Figure S2). The <sup>31</sup>P, <sup>13</sup>C and <sup>1</sup>H NMR spectra (see the Supporting Information) are also compatible with the proposed structures (Scheme 2) and the presence of single species for each compound. Thus, the phosphorus resonances in CD<sub>2</sub>Cl<sub>2</sub> appear in the ranges 22.3–23.4 ppm (aryl-substituted ions) and 20.6–21.5 (methylated ions), which belong to a typical region for other acyclic phosphonium compounds.<sup>[10a,18]</sup> The exchange of the anion



**Scheme 1.** Schematic representation of ESICT-induced anion migration in donor-acceptor ionic dyes in the absence of solvent relaxation (low polarity solvents).



**Scheme 2.** General synthetic routes (A) and structures of donor–acceptor phosphonium salts (B) studied in this work (named  $Y_nZ_{n'}[X]$ , where  $Y$  and  $Z$  correspond to the length of phenylene linkers and the  $n, n'$  subscripts indicate the number of the respective donor-containing substituents).

shows virtually no effect on the chemical shift of the  $^{31}\text{P}$  signal in dichloromethane, indicating weak ion pair association in this solvent. In toluene- $d_8$ , the NMR spectra are substantially more anion-dependent, which can be seen in a non-negligible difference in the  $\delta(^{31}\text{P})$  for triflate and bromide salts (e.g. 21.6 and 22.4 ppm for  $2_1\text{Me}[\text{OTf}]$  and  $2_1\text{Me}[\text{Br}]$ ; 21.1 and 20.7 ppm for  $1_2[OTf]$  and  $1_2[\text{Br}]$ ). The corresponding proton spectra for the selected compounds (Supporting Information) also confirm a non-innocent role of anion in ion pairing in low polarity medium, which has been demonstrated for the family  $2_1[X]$ .<sup>[10a]</sup>

### Photophysical Properties

To avoid complication, we segregate the dyes under study into three groups—*i*) compounds  $2_n[X]$  where we probe the effect of branching the multipolar cations bearing identical substituents; *ii*) quadrupolar compounds containing two elongated  $\pi$ -spacers  $3_2[X]$ , and two different spacers  $Y_1Z_1[X]$  with competing migration pathways; *iii*) methylated species  $2_1\text{Me}[\text{OTf}]$  and  $Y_3\text{Me}[\text{OTf}]$  with sterically and electronically different quaternized phosphorus center.

### Polar Solvents

In polar media such as  $\text{CH}_2\text{Cl}_2$  and  $\text{CH}_3\text{CN}$  one can neglect ion pairing effect due to efficient dissociation. In these solvents, optical properties of all titled salts are not exceptional and arise from intramolecular charge transfer (ICT) transitions expected from the D-A architecture of these cations, being nearly independent on the counterion (Figures S3–S5, Table S1). The absorption profiles of  $2_n[X]$  ( $X^- = \text{Br}^-$ ,  $\text{OTf}^-$ , Figure S3) are close to that of  $2_1[X]$ <sup>[10a]</sup> and display the lowest energy bands around 390–394 nm in  $\text{CH}_2\text{Cl}_2$  (373–378 nm in  $\text{CH}_3\text{CN}$ ), where the molar attenuation coefficient additively grows with the increase of the number  $n$  of the  $-\pi$ -D arms. The structureless emission bands are almost identical for the entire series  $2_n[X]$ . In addition, they all show positive solvatochromism, for which the peak wavelength shifts from 522–528 nm ( $\Phi_{\text{em}} = 0.73$ –0.81) in  $\text{CH}_2\text{Cl}_2$  to 547–551 nm ( $\Phi_{\text{em}} = 0.25$ –0.39) in  $\text{CH}_3\text{CN}$  with moderate to high emission quantum yields. Note that a small hypsochromic shift of the emission maxima for ca. 5 nm is identified within the series of  $2_n^+$  ( $n = 1$ –4) cations, which likely arises from a combination of slight decrease of electron-accepting strength of the phosphonium unit and an

additive effect of the donor-containing substituents. This correlation is further supported by gradually decreasing Stokes shifts (from 6900 cm<sup>-1</sup> for **2**<sub>1</sub>[Br] to 6288 cm<sup>-1</sup> for **2**<sub>4</sub>[Br] in CH<sub>2</sub>Cl<sub>2</sub>, Table S1), and the chemical shifts in the <sup>31</sup>P NMR spectra; the latter indicate slight shielding of the phosphorus nuclei from *n*=1 to *n*=4 (23.5 ppm for **2**<sub>1</sub>, 23.2 ppm for **2**<sub>2</sub>, 22.9 ppm for **2**<sub>3</sub>, 22.6 ppm for **2**<sub>4</sub>). Very close fluorescence spectral properties of **2**<sub>*n*</sub>[X] in dichloromethane and acetonitrile suggest that the corresponding electronic transitions mostly occur within one {<sup>+</sup>P-(C<sub>6</sub>H<sub>4</sub>)<sub>2</sub>-NPh<sub>2</sub>} push-pull arm, i.e. there is no appreciable electronic coupling between A<sup>+</sup>-D subchromophores in A<sup>+</sup>(-D)<sub>*n*</sub> (*n*=2-4) multipolar ions, which can be approximated in polar solvents as chromophores with dipolar symmetry-broken excited state.<sup>[19]</sup> Optimization of the S<sub>0</sub> geometry for the cation **2**<sub>2</sub><sup>+</sup> with density functional theory (DFT) leads in a geometry where both biphenylene spacers are somewhat twisted with estimated torsion angle of about 30°. The lowest energy absorption S<sub>0</sub>(optimized)→S<sub>1</sub> in **2**<sub>2</sub><sup>+</sup> involves two equivalent chromophore arms and results in substantial charge transfer from the donor -NPh<sub>2</sub> motifs as well as changing polarization of the π-spacer (Figure 1). At the optimized S<sub>1</sub> geometry, one -(C<sub>6</sub>H<sub>4</sub>)<sub>2</sub>-NPh<sub>2</sub> fragment becomes flattened and is responsible for the emission that makes **2**<sub>2</sub><sup>+</sup> behaving in a dipolar manner.

In CH<sub>2</sub>Cl<sub>2</sub> and CH<sub>3</sub>CN, the behavior of salts **3**<sub>2</sub>[X], **1**<sub>1</sub>**3**<sub>1</sub>[X] and **2**<sub>1</sub>**3**<sub>1</sub>[X] (X<sup>-</sup>=Br<sup>-</sup>, OTf<sup>-</sup>) is dominated by the -π-D fragment with terphenylene spacer (Figure S4 and Table S1). The non-symmetric cations **1**<sub>1</sub>**3**<sub>1</sub><sup>+</sup> and **2**<sub>1</sub>**3**<sub>1</sub><sup>+</sup> reveal minor hypsochromic shifts of yellow-orange emission, and substantially higher quantum yields (Φ<sub>em</sub>=0.77/0.66 in CH<sub>2</sub>Cl<sub>2</sub>, 0.32/0.15 in CH<sub>3</sub>CN) than **3**<sub>2</sub><sup>+</sup> congener (Φ<sub>em</sub>=0.30 in CH<sub>2</sub>Cl<sub>2</sub>, 0.06 in CH<sub>3</sub>CN). The lack of dual fluorescence

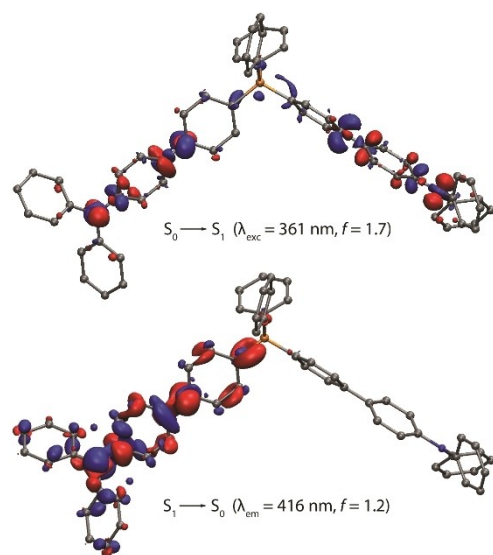


**Figure 1.** Lowest energy excitation S<sub>0</sub>→S<sub>1</sub> and emission S<sub>1</sub>→S<sub>0</sub> electron density difference plots for cation **2**<sub>2</sub><sup>+</sup> (isovalue 0.002 a.u., DFT-LRC-ωPBEh method, optimized S<sub>0</sub> and S<sub>1</sub> geometries). During the electronic transition, the electron density increases in the blue areas and decreases in the red areas. Hydrogen atoms and counter anions are omitted for clarity.

for **1**<sub>1</sub>**3**<sub>1</sub><sup>+</sup> and **2**<sub>1</sub>**3**<sub>1</sub><sup>+</sup> in polar media is in line with Kasha's rule, i.e. the emission is associated with the dipolar lowest excited state, which corresponds to the ICT occurring on the arm with the longest terphenylene spacer. The DFT-calculated electronic transitions S<sub>0</sub>→S<sub>1</sub>/S<sub>0</sub>←S<sub>1</sub> in cation **2**<sub>1</sub>**3**<sub>1</sub><sup>+</sup> obtained for symmetry unconstrained geometries (C<sub>1</sub>) primarily involve the shorter chromophore component, which becomes flattened during the geometry optimization of the S<sub>1</sub> state (Figure S5). However, considering an average conformation (C<sub>s</sub>) with flattened phenylene spacers on both chromophores shifts the localization of electronic transitions related to the excitation/emission mainly to the terphenylene fragment. The C<sub>s</sub> structure is energetically higher than the C<sub>1</sub> local minimum by only 10 kJ mol<sup>-1</sup> per phenylene group, making the C<sub>s</sub> structure an energetically feasible idealized description of the molecular conformation in solution.

The absorption and emission signals of the methylated dyes **2**<sub>1</sub>**Me**[OTf], **2**<sub>3</sub>**Me**[OTf] and **3**<sub>3</sub>**Me**[OTf] in CH<sub>2</sub>Cl<sub>2</sub> and CH<sub>3</sub>CN demonstrate modest hypsochromic shifts with respect to their tetraarylated relatives (Figure S6 and Table S1). Apparently, this energy increase, which is more pronounced in more polar acetonitrile, is caused by non-electron accepting methyl substituent and therefore less polarizing effect of the phosphonium group.

### Non-polar Solvents

*i) Multipolar dyes **2**<sub>*n*</sub>[X] (*n*=2-4; X<sup>-</sup>=Br<sup>-</sup>, OTf<sup>-</sup>)* In the lower polarity solvent such as toluene, where ion pairing is anticipated, branching the molecular structure of the phosphonium cations has a distinct influence on the photoluminescence characteristics. In accordance with earlier studies,<sup>[10a]</sup> new fluorophores **2**<sub>*n*</sub>[X] demonstrate high-energy (HiE, F<sub>1</sub>) and low-energy (LoE, F<sub>2</sub>) emission bands of variable ratio in their steady-state spectra (Table 1, Figures 2 and S7). The excitation spectra recorded for F<sub>1</sub> and F<sub>2</sub> emission bands for all **2**<sub>*n*</sub>[X] (Figure S8) are identical with the absorption profiles, confirming that they both share common ground-state species. By analogy with **2**<sub>1</sub><sup>+</sup>, the F<sub>1</sub> band is assigned to an anion-destabilized ICT state S<sub>1</sub>, whereas the red-shifted F<sub>2</sub> band emerges upon photoinduced anion migration and consequent stabilization of the initial charge separated state (S<sub>1</sub>' , Scheme 1). The emission spectra of **2**<sub>2</sub>[OTf] in frozen toluene and dichloromethane solutions at 77 K display only the blue shifted HiE signals (Figure S9). The results imply completely suppressed anion migration in frozen ion pair, which is electrostatically stabilized in the ground state but destabilized in the CT excited state.

Due to higher stability, triflate salts were used for most of time-resolved studies. Transient emission spectra monitored in the 0.1-1.0 ns time range for **2**<sub>*n*</sub>[OTf] (*n*=2-4; Figures 2 and S7) reveal that the initial HiE F<sub>1</sub> band, recorded at 0.1 ns delay after the excitation pulse, undergoes continuous transformation into the LoE F<sub>2</sub> fluorescence, which is completed within 0.8-1.0 ns. The spectral temporal evolution of red-shifted emission correlates well with the kinetics of the F<sub>2</sub> band, for which a rise component of ca. 170 ps can be resolved by time-correlated single photon

**Table 1:** Photophysical data of the studied phosphonium salts in toluene at 298 K.

Cation	Anion A <sup>-</sup>	$\lambda_{\text{abs}}$ [nm]	$\lambda_{\text{em}}$ [nm]	$F_1/F_2$ <sup>[a]</sup>	$\Phi_{\text{em}}$	$\tau_{F_1}$ [ps] (prefactor) <sup>[b]</sup>	$\tau_{F_2}$ [ps] (prefactor) <sup>[b]</sup>	CIE
<b>2<sub>1</sub></b> <sup>[10a]</sup>	Br <sup>-</sup>	379	468, 592sh	1/0.41	0.17	67 (0.63), 450 (0.37)	93 (-0.49), 792 (0.36), 2439 (0.15)	0.29, 0.34
	OTf <sup>-</sup>	383	468, 589	0.39/1	0.47	150 (0.73), 660 (0.27)	298 (-0.45), 3807 (0.55)	0.42, 0.43
<b>2<sub>2</sub></b>	Br <sup>-</sup>	380	468, 586	0.57/1	0.15	70 (0.95), 350 (0.05)	95 (-0.51), 648 (0.36), 2058 (0.13)	0.39, 0.41
	OTf <sup>-</sup>	385	468, 586	0.29/1	0.38	111 (0.99), 2741 (0.01)	185 (-0.51), 3306 (0.49)	0.42, 0.45
<b>2<sub>3</sub></b>	Br <sup>-</sup>	382	468, 584	0.60/1	0.15	71 (0.99), 605 (0.01)	97 (-0.48), 610 (0.33), 1983 (0.19)	0.39, 0.41
	OTf <sup>-</sup>	386	468, 584	0.30/1	0.34	90 (0.99), 2362 (0.01)	163 (-0.51), 2904 (0.49)	0.43, 0.45
<b>2<sub>4</sub></b>	Br <sup>-</sup>	383	468, 582	0.69/1	0.10	65 (0.98), 1037 (0.02)	112 (-0.50), 550 (0.31), 1669 (0.19)	0.38, 0.40
	OTf <sup>-</sup>	386	468, 580	0.35/1	0.30	79 (0.99), 2285 (0.01)	171 (-0.49), 2627 (0.51)	0.42, 0.44
<b>3<sub>1</sub></b>	Br <sup>-</sup> <sup>[10a]</sup>	373	480, 660	1/0.18	0.17	120 (0.39), 780 (0.61)	120 (-0.39), 2540 (0.61)	0.21, 0.29
	OTf <sup>-</sup>	372	482, 661	1/0.64	0.42	80 (0.52), 782 (0.48)	405 (-0.38), 3600 (0.62)	0.31, 0.34
<b>3<sub>2</sub></b>	Br <sup>-</sup>	375	480, 665	1/0.29	0.19	118 (0.36), 470 (0.64)	118 (-0.46), 1971 (0.64)	0.24, 0.30
	OTf <sup>-</sup>	375	481, 664	1/0.84	0.29	93 (0.37), 466 (0.63)	290 (-0.46), 3433 (0.54)	0.34, 0.34
<b>1<sub>1,2</sub></b>	Br <sup>-</sup>	370	470, 570	1/0.80	0.17	86 (0.74), 500 (0.25), 2798 (0.01)	105 (-0.51), 938 (0.27), 3385 (0.22)	0.32, 0.35
	OTf <sup>-</sup>	371	470, 576	0.60/1	0.53	93 (0.55), 637 (0.43), 3381 (0.02)	424 (-0.47), 4043 (0.53)	0.38, 0.41
<b>1<sub>1,3</sub></b>	Br <sup>-</sup>	361	473, 645	1/0.30	0.21	115 (0.73), 761 (0.27)	90 (-0.50), 1520 (0.27), 2694 (0.23)	0.25, 0.28
	OTf <sup>-</sup>	361	471, 642	1/0.55	0.49	85 (0.53), 1012 (0.47)	520 (-0.44), 3908 (0.56)	0.30, 0.31
<b>2<sub>1,3</sub></b>	Br <sup>-</sup>	377	477, 615	1/0.48	0.09	65 (0.55), 237 (0.44), 1536 (0.01)	121 (-0.49), 769 (0.27), 1806 (0.24)	0.29, 0.32
	OTf <sup>-</sup>	378	480, 613	0.66/1	0.23	65 (0.45), 248 (0.54), 2707 (0.01)	197 (-0.50), 3262 (0.50)	0.40, 0.40
<b>2<sub>1</sub>Me</b>	OTf <sup>-</sup>	378	465, 583	1/0.52	0.53	604 (0.87), 3477 (0.13)	657 (-0.49), 3602 (0.51)	0.29, 0.31
<b>2<sub>3</sub>Me</b>	OTf <sup>-</sup>	380	461, 573	1/0.55	0.62	439 (0.89), 2700 (0.11)	643 (-0.49), 3225 (0.51)	0.29, 0.31
<b>3<sub>3</sub>Me</b>	OTf <sup>-</sup>	371	473, 650	1/0.12	0.79	1088 (0.95), 2350 (0.05)	1496 (-0.44), 3264 (0.56)	0.20, 0.27

[a] The  $F_1/F_2$  ratio was calculated using the intensities of the emission spectra at the maxima of the  $F_1$  and  $F_2$  bands. [b] Measured at the 440 ( $\tau_{F_1}$ ) and 640/660 nm ( $\tau_{F_2}$ ) for **2/3** containing cations.

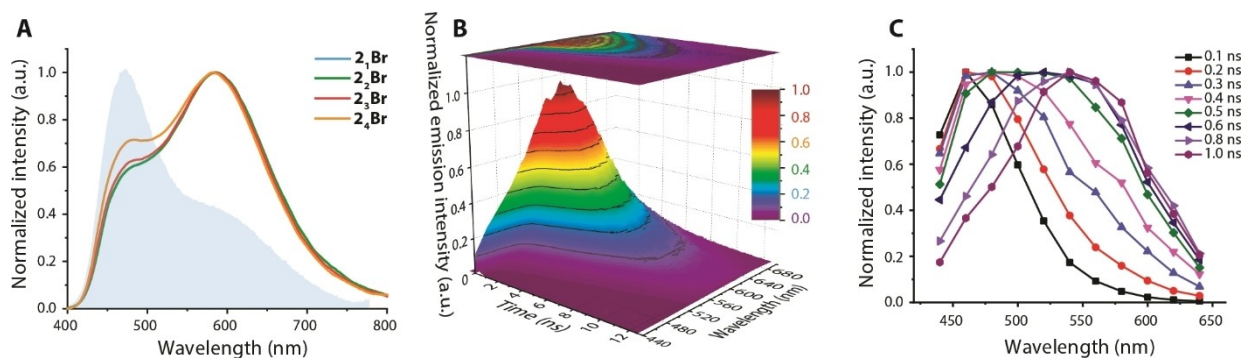


**Figure 2.** A) Normalized emission spectra of **2<sub>n</sub>**[Br] (filled graph corresponds to **2<sub>1</sub>**[Br]<sup>[10a]</sup>). B), C) Time-resolved emission spectra of **2<sub>2</sub>**[OTf] in toluene at 298 K.

counting (TCSPC) measurements, followed by the relaxation of the excited state with  $\tau_{\text{obs}}=2.6\text{--}3.3$  ns (Table 1, Figure S9).

Triflate salts demonstrate systematically higher quantum yields ( $\Phi_{\text{em}}=0.47\text{--}0.30$ ) than the bromide congeners ( $\Phi_{\text{em}}=0.17\text{--}0.10$ ), while the multipolar dyes show somewhat lower intensity than dipolar compounds. The transition from dipolar (D–A<sup>+</sup>) **2<sub>1</sub>**<sup>+</sup> to quadrupolar (D–A<sup>+</sup>–D) **2<sub>2</sub>**<sup>+</sup> architecture in the presence of Br<sup>-</sup> anion dramatically increases the intensity of  $F_2$  band ( $\lambda=586$  nm) relative to  $F_1$  band ( $\lambda=468$  nm) that changes the  $F_1/F_2$  ratio from 1/0.41 to 0.57/1 (Figure 2 and Table 1) but retains both the emission wavelengths and the total quantum yields ( $\Phi_{\text{em}}=0.17$  and 0.15 for **2<sub>1</sub>**[Br] and **2<sub>2</sub>**[Br]). Qualitatively, the same trend is observed for OTf<sup>-</sup> salts, for which the LoE signal dominates and grows for **2<sub>2</sub>**<sup>+</sup> vs **2<sub>1</sub>**<sup>+</sup> cation (Figure S7). Schematically, it can be illustrated by the symmetrically branched molecular

structure of **2<sub>2</sub>**<sup>+</sup> that increases the probability of photo-induced anion translocation by providing two accessible migration pathways and minimizing steric restrictions, i.e. eliminating migration-unfavorable locations for relatively small counterions around the cationic motif (Figure 3). An additional enhancement of migration can be offered by the quadrupolar excited state, which might have an appreciable contribution in non-polar solvents.<sup>[19d]</sup>

Further addition of the subchromophores to the phosphorus atom in **2<sub>3</sub>**<sup>+</sup> and **2<sub>4</sub>**<sup>+</sup> slightly raises both the emission energy of the  $F_2$  band, and the intensity of the  $F_1$  band (Figures 2A and S7A, Table 1). The subsequent increase of the number of equivalent  $-\pi$ -D arms in **2<sub>3</sub>**<sup>+</sup> and **2<sub>4</sub>**<sup>+</sup> is not expected to improve significantly steric conditions for anion migration compared to those in **2<sub>2</sub>**<sup>+</sup>. This supposition correlates with close rise times for the  $F_2$  band among multipolar **2<sub>n</sub>**[OTf] species ( $n=2\text{--}4$ ,

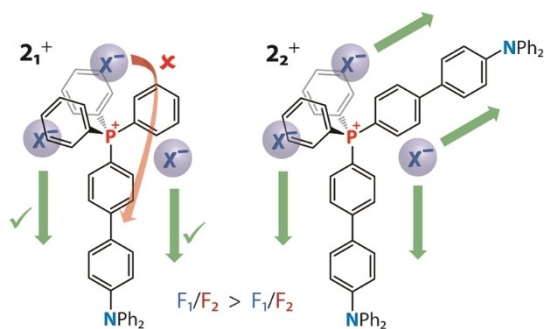


**Figure 3.** Schematic representation of the effect of dipolar and quadrupolar architectures on the possibility of anion migration.

with a rise component of  $\tau_{F_2}$  of 163–185 ps). Possible delocalization of the CT excited state over three ( $2_3^+$ ) and four ( $2_4^+$ ) sites might somewhat decrease the depletion of electron density from the  $\text{NPh}_2$  groups with respect to dipolar compounds. This should disfavor the Coulomb attraction  $\text{X}^- \cdots \delta^+\text{NPh}_2$  in the charge-separated states (Scheme 1 and Figure 3), and therefore slightly diminish the efficiency of anion migration and the intensity of  $F_2$  band.

ii) *Quadrupolar dyes*  $3_2[A]$ ,  $1_1 2_1[A]$ ,  $1_1 3_1[A]$ ,  $2_1 3_1[A]$  ( $A^- = \text{Br}^-, \text{OTf}^-$ ) Taking into account that major alterations of luminescence for  $2_n^+$  series are observed between the a) dipolar and quadrupolar ions, and b) different counterions, in the next stage we explore the tunability of the emission among the quadrupolar  $\text{D}-\text{A}^+-\text{D}$  and  $\text{D}-\text{A}^+-\text{D}'$  type of dyes. As we have shown for salts  $2_1[\text{Br}]$  and  $3_1[\text{Br}]$ ,<sup>[10a]</sup> elongation of the  $\pi$ -spacer from biphenylene to terphenylene insignificantly red shifts the  $F_1$  band (from 468 to 480 nm), but has a more drastic effect on the  $F_2$  signal, increasing its wavelength from 592 to 660 nm that is accompanied by a drop of its intensity to produce sky-blue fluorescence. Quadrupolar configuration of  $3_2[\text{Br}]$  enhances the  $F_2$  band (the  $F_1/F_2$  ratio varies from 1/0.18 for  $3_1[\text{Br}]$  to 1/0.29, Figure 4). In line with the behavior of  $2_n[\text{X}]$ , the intensity of the LE band for  $3_2^+$  demonstrates further growth upon exchange of the  $\text{Br}^-$  for the  $\text{OTf}^-$  counterion ( $F_1/F_2 = 1/0.84$  for  $3_2[\text{OTf}]$ ). This results in nearly pure white light emission demonstrated by  $3_2[\text{OTf}]$ , Commission Internationale de l'Éclairage (CIE) coordinates (0.34, 0.34), with good quantum yield of 0.29 (Table 1).

The hypothesis of photoinduced anion migration that is responsible for temporal growth of the LoE band, initially elaborated for  $2_n^+$  series, is applicable to the dyes with longer terphenylene  $\pi$ -spacers. Similar to  $2_n^+$ , for the  $3_n^+$  series, the identity of the excitation spectra monitored in the range of the emission from 450 to 700 nm for salts containing  $-(\text{C}_6\text{H}_4)_3-\text{NPh}_2$  fragment (Figure S10) points to the common origin of the  $F_1$  and  $F_2$  fluorescence bands. Time-resolved data (Figures 4 and S11) also fit well the proposed concept and confirm the rise of red shifted  $F_2$  signal that follows the initially developed HiE band.

Combination of two different chromophores in cations  $1_1 2_1^+$ ,  $1_1 3_1^+$  and  $2_1 3_1^+$  has little influence on their emission in polar solvents compared to that of individual species  $2_1^+$  and  $3_1^+$  (see above, Figures S3 and S4), which is dominated by the longest  $-\pi-\text{D}$  fragment. Contrarily, in toluene these asymmetric dyes exhibit the contribution of both components into the total steady state luminescence (Figures S12–S14). For detailed analyses we have chosen salt  $2_1 3_1[\text{OTf}]$ , the emission spectrum of which is shown in Figure 5. Its spectral profile suggests the presence of two active migration pathways along two different  $-\pi-\text{D}$  arms and may be seen as a superposition of those of dipolar dyes  $2_1[\text{OTf}]$  and  $3_1[\text{OTf}]$ . Due to similarity of HiE bands of the latter compounds (468 and 482 nm), the experimental spectrum of  $2_1 3_1[\text{OTf}]$  can be fitted with three components, which correspond to the average  $F_1$  and two migration-induced LoE bands ( $F_2$  and  $F_2'$ ) assigned to the  $-\text{biphenylene}-\text{NPh}_2$  (**2**) and  $-\text{terphenylene}-\text{NPh}_2$  (**3**) motifs (Figure 5B). Time-dependent emission spectra of  $2_1 3_1[\text{OTf}]$  (Figure 5C) also support this process of competing migration, and clearly display the appearance of the intermediate  $F_2$  signal around 575 nm, which occurs in a faster time scale than  $F_2'$  and is absent for  $3_n[\text{OTf}]$  congeners (Figure 4).

The possibility of such anion motion in two non-equivalent directions in the ion pair of  $2_1 3_1[\text{OTf}]$  is tentatively ascribed to the excitation of both constituting chromophores having close energies (Figure S5). Possible delocalization of the  $S_1$  state over the entire cation or the contribution of two dipolar excited configurations (i.e.  $2_1^* 3_1^+$  and  $2_1 3_1^{*+}$ ) should provide two opportunities for anion migration and therefore lead to the evolution of two red shifted bands,  $F_2$  and  $F_2'$ . Two other non-symmetrical salts,  $1_1 2_1[\text{OTf}]$  and  $1_1 3_1[\text{OTf}]$ , generally operate pursuant to

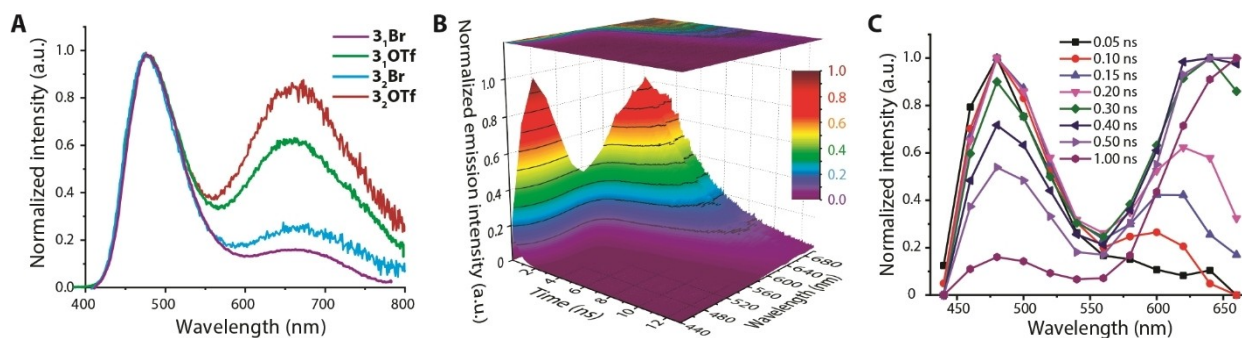


**Figure 4.** A) Normalized emission spectra of  $3_n[\text{X}]$  ( $n=1, 2$ ;  $\text{A}^- = \text{Br}^-, \text{OTf}^-$ ). B), C) Time-resolved emission spectra of  $3_2[\text{OTf}]$  in toluene at 298 K.

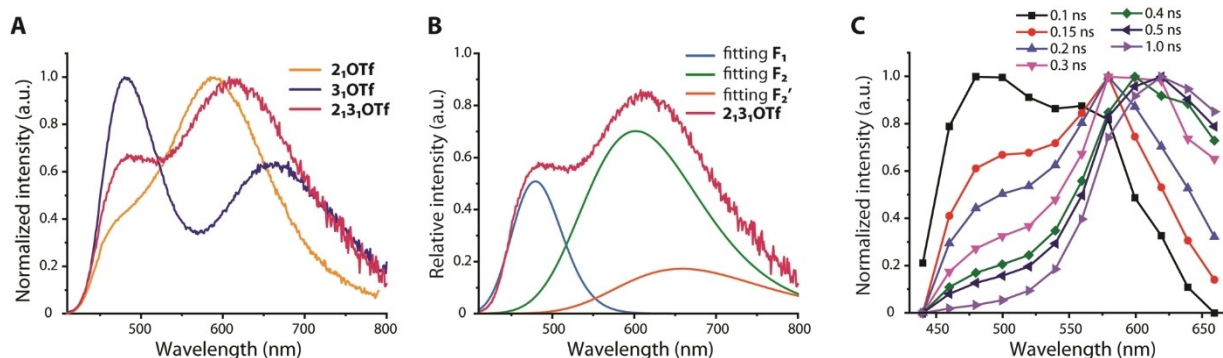


**Figure 5.** A) Comparison of normalized emission spectra of  $2_1$ [OTf],  $3_1$ [OTf] and  $2_13_1$ [OTf]. B) Simulated deconvolution of the emission spectrum of  $2_13_1$ [OTf] into three components (one HiE  $F_1$  and two migration-induced  $F_2$  and  $F_2'$  bands). C) Time-resolved emission spectra of  $2_13_1$ [OTf]; toluene, 298 K.

$2_13_1$ [OTf]. Their LoE bands are slightly blue shifted relative to  $2_1$ [OTf] and  $3_1$ [OTf], respectively (Figure S12). The short  $-\text{phenylene}-\text{NPh}_2$  (**1**) group, the emission of which is poorly responsive to anion migration,<sup>[10a]</sup> evidently causes the growth of the  $F_1$  signal in  $1_12_1$ [OTf] and  $1_13_1$ [OTf]. On the other hand, in contrast to  $2_2$ [OTf] ( $\Phi_{\text{em}}=0.38$ ),  $2_13_1$ [OTf] ( $\Phi_{\text{em}}=0.23$ ) and  $3_2$ [OTf] ( $\Phi_{\text{em}}=0.29$ ), branching the dipolar phosphonium ions with chromophore **1** does not have a detrimental effect on the quantum yields, which in the case of  $1_12_1$ [OTf] ( $\Phi_{\text{em}}=0.53$ ) and  $1_13_1$ [OTf] ( $\Phi_{\text{em}}=0.49$ ) slightly exceed those of  $2_1$ [OTf] ( $\Phi_{\text{em}}=0.47$ ) and  $3_1$ [OTf] ( $\Phi_{\text{em}}=0.42$ , Table 1).

iii) *Methylated dyes  $2_1\text{Me}$ [OTf],  $2_3\text{Me}$ [OTf] and  $3_3\text{Me}$ [OTf].* Tuning the electron deficient nature of the phosphonium group and its polarizing ability toward the  $-\pi$ -D motifs envisages the variation of the environment around the phosphorus atom. In this approach, the methylated derivatives  $2_1\text{Me}$ [OTf],  $2_3\text{Me}$ [OTf] and  $3_3\text{Me}$ [OTf] were selected to probe the effect of electronic and steric features of the  $-\text{PR}_3$  moiety on their optical properties. Accordingly, the electron deficiency of the phosphonium group can be directly identified by the chemical shift from the  $^{31}\text{P}$  NMR spectrum (see above). The replacement of the phenyl in cations  $2_1^+$  and  $2_3^+$  for the electron-donating methyl substituent leads to upfield shift of the phosphorus resonances from 22.3–23.4 ppm (tetraaryl-substituted ions)

to 20.6–21.5 ppm (methylated ions). Surprisingly, this simple modification of the phosphonium group transforms yellowish emission of the tetraaryl triflates  $2_1$ [OTf] and  $2_3$ [OTf] with dominating LoE band ( $F_1/F_2=0.39/1$  and  $0.30/1$ , CIE 0.42,0.43 and 0.43,0.45) into cold white-blueish luminescence of the methylated congeners  $2_1\text{Me}$ [OTf] and  $2_3\text{Me}$ [OTf] with predominant HiE band ( $F_1/F_2=1/0.52$  and  $1/0.55$ , CIE 0.29,0.31) (Figure 6). Further, the largest quantum yield ( $\Phi_{\text{em}}=0.62$ ) is achieved for multipolar configuration of  $2_3\text{Me}$ [OTf], which is opposite to arylated cations exhibiting the highest intensities among the dipolar compounds.

The time-resolved spectra (Figures 6B and S15) unequivocally indicate considerably slower evolution of  $F_2$  band for  $2_1\text{Me}$ [OTf] and  $2_3\text{Me}$ [OTf] that correlates with much longer rise times of this LoE signal (657 and 643 ps, Figure S16 and Table 1) in comparison with those of  $2_1$ [OTf] and  $2_3$ [OTf] (298 and 163 ps, Table 1). Within the framework of our hypothesis, such spectroscopic features propound less efficient anion migration for methyl-containing cations. Tentatively, we attribute the phenomenon to the combination of steric and polarization effects induced by the methyl group. In the  $S_0$  state (no solvation model applied), the dipole moment of  $2_1\text{Me}^+$  (13.8 D) is visibly larger than that of  $2_1^+$  (11.9 D). This is in line with ca. 30 kJ mol $^{-1}$  higher ion pairing energy predicted for the optimized structures of  $2_1\text{Me}$ [OTf] and  $2_2$ [OTf]. In the excited  $S_1$  state, the dipole

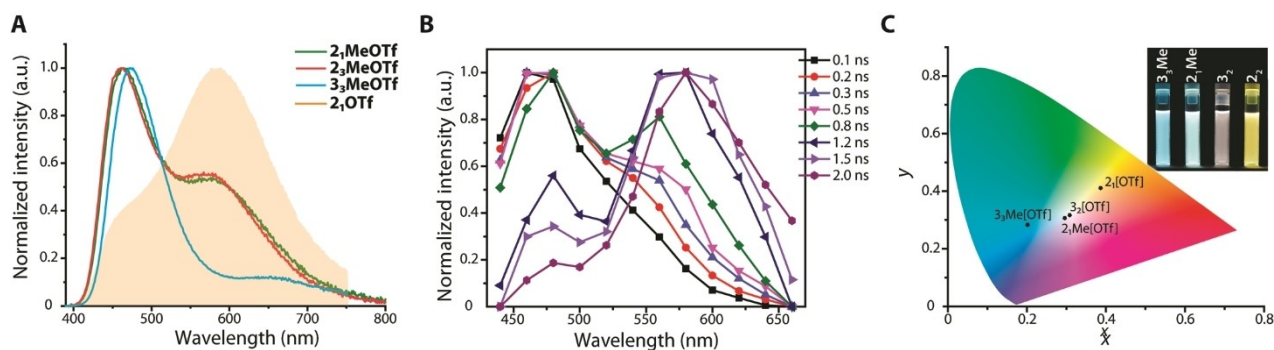


**Figure 6.** A) Normalized emission spectra of  $2_1\text{Me}$ [OTf],  $2_3\text{Me}$ [OTf] and  $3_3\text{Me}$ [OTf] (filled graph corresponds to  $2_1$ [OTf]<sup>[10a]</sup>). B) Time-resolved emission spectra of  $2_1\text{Me}$ [OTf]. C) CIE 1931 coordinates for  $2_1$ [OTf],  $2_1\text{Me}$ [OTf],  $3_2$ [OTf] and  $3_3\text{Me}$ [OTf]; toluene, 298 K.

moment of  $\mathbf{2}_1^+$  and  $\mathbf{2}_1\text{Me}^+$  decreases to 1.7 D and 4.3 D, respectively. This implies a somewhat smaller charge redistribution for  $\mathbf{2}_1\text{Me}^+$  compared to that for  $\mathbf{2}_1^+$  in the  $S_1$  state and could result in a less favourable anion migration along the  $\mathbf{2}_1\text{Me}^+$  cation. Consequently, the system undergoes radiative relaxation primarily from charge destabilized  $S_1$  state (Scheme 1) producing predominant HiE fluorescence. The smaller bromide anion in  $\mathbf{2}_1\text{Me}[\text{Br}]$  reveals further decrease in the intensity of the  $F_2$  band (Figure S19), which generally supports the hypothesis. We have optimized the  $S_0$  geometry for salts  $\mathbf{2}_1\text{Me}[\text{Br}]$  and  $\mathbf{2}_1[\text{Br}]$ , see Supporting Information. In both cases the bromide anion shows attractive interactions with the H atoms of the phenyl or methyl fragments, which seem to be stronger for  $\text{H}(\text{Me})\cdots\text{Br}$  contact thanks to higher polarization of the Me. These secondary interactions remain in the CT state and further hinder the movement of the anion for methylated cations. The terphenylene-based compound  $\mathbf{3}_3\text{Me}[\text{OTf}]$  adheres the same tendency, manifested by a substantially decreased intensity of the  $F_2$  band ( $F_1/F_2=1/0.12$ , CIE 0.20, 0.27) and additional growth of its rise time as long as 1496 ps.

## Conclusion

In summary, via utilizing the unique organophosphonium motif, which chemically combines versatile connectivity of the quaternized phosphorus atom with pronounced electron-deficient properties, we have prepared a series of multipolar donor-acceptor ionic dyes ( $(\text{D}-\pi-)_n\text{A}^+[\text{X}^-]$  ( $\text{D}=\text{NPh}_2$ ,  $\text{A}^+=^+\text{PR}_{4-n}$  derivative) to investigate the effect of molecular structure on the photophysical behavior in relation to the counterion migration proposed for non-dissociated ion pairs in solvents of low polarity. For this purpose, we varied the amount of the constituting chromophores around the P center  $^+\text{PPh}_{4-n}(-\pi-\text{D})_n$  ( $n=1-4$ ,  $\pi=-\text{(C}_6\text{H}_4)_x-$ ), combined two different donor-acceptor arms  $^+\text{PPh}_2(-\pi-\text{D})(-\pi'-\text{D})$  in the same cation, and changed the steric and electronic features of the phosphonium fragment in methylated species  $^+\text{PMePh}_{3-m}(-\pi-\text{D})_m$  ( $m=1, 3$ ). In polar solvents (dichloromethane, acetonitrile), the new compounds reveal regular fluorescence with positive solvatochromism, virtually independent on the branching of the dye cation and assigned to dipolar-like intramolecular charge transfer (ICT) excited state, which originates primarily from the  $-\pi-\text{D}$  component with the largest  $\pi$ -spacer. In lower polarity medium (toluene), all salts are expected to exist as ion pairs and exhibit spectral temporal evolution of multiple emissions shifting from blue to red region. The resulting steady-state panchromatic luminescence is associated with continuous electrostatic stabilization of the excited state upon anion migration from the ground-state location in the direction opposite to that of ICT. In the ion paired form, the transition from dipolar to quadrupolar molecular structure substantially enhances the low energy band due to stereochemical reasons by providing the additional migration pathways. The quadrupolar architecture together with the adjustable lengths of the  $\pi$ -spacers, and the nature of counterions allow for efficient tuning of the emission and

achieving nearly pure white light with appreciable quantum yields. On the other hand, introducing the methyl substituent to the phosphorus atom dramatically reduces the rate of ion migration and suppresses the red shifted bands simultaneously improving total emission intensity. The presented results thus point to a quite general character of fast photoinduced anion motion that occurs in ion-paired dyes and is accompanied by the optical response. This multiple intra-ion-pair dynamics and the corresponding fluorescence response can be rationally fine-tuned on the molecular level that might considerably broaden the scope of functionalities and stimulate the development of new ionic systems for molecular machinery.

## Experimental Section

Synthetic, other experimental and computational details (PDF) are given in the Supporting Information.

## Acknowledgements

P.-T.C. appreciates the Ministry of Science and Technology, Taiwan, for generous supports. I.O.K. acknowledges the Academy of Finland (decision 317903, I.O.K.; Flagship Programme, Photonics Research and Innovation PREIN, decision 320166). A.J.K. thanks the Finnish IT Center for Science (CSC) for computational resources. A.B. is grateful to Jenny and Antti Wihuri Foundation for a post-doctoral grant.

## Conflict of Interest

The authors declare no conflict of interest.

## Data Availability Statement

The data that support the findings of this study are available in the Supporting Information of this article.

**Keywords:** Charge Transfer · Donor–Acceptor Systems · Dual Emission · Ion Pairs · Phosphonium

- [1] a) H. K. Bisoyi, Q. Li, *Chem. Rev.* **2016**, *116*, 15089–15166; b) Q. Yu, B. Aguila, J. Gao, P. Xu, Q. Chen, J. Yan, D. Xing, Y. Chen, P. Cheng, Z. Zhang, S. Ma, *Chem. Eur. J.* **2019**, *25*, 5611–5622; c) W.-C. Xu, S. Sun, S. Wu, *Angew. Chem. Int. Ed.* **2019**, *58*, 9712–9740; *Angew. Chem.* **2019**, *131*, 9814–9843; d) X. Pang, J.-a. Lv, C. Zhu, L. Qin, Y. Yu, *Adv. Mater.* **2019**, *31*, 1904224; e) B. L. Feringa, *Adv. Mater.* **2020**, *32*, 1906416.
- [2] a) D. Roke, S. J. Wezenberg, B. L. Feringa, *Proc. Natl. Acad. Sci. USA* **2018**, *115*, 9423; b) D. Dattler, G. Fuks, J. Heiser, E. Moulin, A. Perrot, X. Yao, N. Giuseppone, *Chem. Rev.* **2020**, *120*, 310–433; c) V. García-López, D. Liu, J. M. Tour, *Chem. Rev.* **2020**, *120*, 79–124.

- [3] a) S. Silvi, M. Venturi, A. Credi, *Chem. Commun.* **2011**, 47, 2483–2489; b) M. Baroncini, S. Silvi, A. Credi, *Chem. Rev.* **2020**, 120, 200–268.
- [4] S. Saha, J. F. Stoddart, *Chem. Soc. Rev.* **2007**, 36, 77–92.
- [5] a) A. M. Brouwer, C. Frochot, F. G. Gatti, D. A. Leigh, L. c Mottier, F. Paolucci, S. Roffia, G. W. H. Worpel, *Science* **2001**, 291, 2124–2128; b) V. Balzani, M. Clemente-León, A. Credi, B. Ferrer, M. Venturi, A. H. Flood, J. F. Stoddart, *Proc. Natl. Acad. Sci. USA* **2006**, 103, 1178–1183.
- [6] T. Kumpulainen, M. R. Panman, B. H. Bakker, M. Hilbers, S. Woutersen, A. M. Brouwer, *J. Am. Chem. Soc.* **2019**, 141, 19118–19129.
- [7] E. Y. Chernikova, D. V. Berdnikova, Y. V. Fedorov, O. A. Fedorova, F. Maurel, G. Jonusauskas, *Phys. Chem. Chem. Phys.* **2017**, 19, 25834–25839.
- [8] a) B. Valeur, I. Leray, L. Zhao, V. Souchon, R. Métivier, P. Plaza, C. Ley, F. Lacombat, M. M. Martin, *ChemPhysChem* **2010**, 11, 2416–2423; b) N. Dozova, R. Kumar, T. Pradhan, F. Lacombat, B. Valeur, J. S. Kim, P. Plaza, *Chem. Commun.* **2015**, 51, 14859–14861.
- [9] a) M. L. Horng, K. Dahl, G. Jones, M. Maroncelli, *Chem. Phys. Lett.* **1999**, 315, 363–370; b) P. M. Pithan, D. Decker, M. S. Sardo, G. Viola, H. Ihmels, *Beilstein J. Org. Chem.* **2016**, 12, 854–862.
- [10] a) A. Belyaev, Y.-H. Cheng, Z.-Y. Liu, A. J. Karttunen, P.-T. Chou, I. O. Koshevoy, *Angew. Chem. Int. Ed.* **2019**, 58, 13456–13465; *Angew. Chem.* **2019**, 131, 13590–13599; b) T.-C. Lin, Z.-Y. Liu, S.-H. Liu, I. O. Koshevoy, P.-T. Chou, *JACS Au* **2021**, 1, 282–293.
- [11] A. Belyaev, P.-T. Chou, I. O. Koshevoy, *Chem. Eur. J.* **2021**, 27, 537–552.
- [12] a) L. Horner, U. M. Duda, *Tetrahedron Lett.* **1970**, 11, 5177–5181; b) D. Marcoux, A. B. Charette, *Adv. Synth. Catal.* **2008**, 350, 2967–2974.
- [13] A. Belyaev, S. O. Slavova, I. V. Solovyev, V. Sizov, J. Jänis, E. V. Grachova, I. O. Koshevoy, *Inorg. Chem. Front.* **2020**, 7, 140–149.
- [14] I. Kondrasenko, Z.-H. Tsai, K.-y. Chung, Y.-T. Chen, Y. Y. Ershova, A. Doménech-Carbó, W.-Y. Hung, P.-T. Chou, A. J. Karttunen, I. O. Koshevoy, *ACS Appl. Mater. Interfaces* **2016**, 8, 10968–10976.
- [15] a) X. Yang, Y. Zhao, X. Zhang, R. Li, J. Dang, Y. Li, G. Zhou, Z. Wu, D. Ma, W.-Y. Wong, X. Zhao, A. Ren, L. Wang, X. Hou, *J. Mater. Chem.* **2012**, 22, 7136–7148; b) Z. H. Li, M. S. Wong, Y. Tao, M. D'Iorio, *J. Org. Chem.* **2004**, 69, 921–927.
- [16] D. Marcoux, A. B. Charette, *J. Org. Chem.* **2008**, 73, 590–593.
- [17] W. Huang, C.-H. Zhong, *ACS Omega* **2019**, 4, 6690–6696.
- [18] a) M. H. Lee, T. Agou, J. Kobayashi, T. Kawashima, F. P. Gabbai, *Chem. Commun.* **2007**, 1133–1135; b) Y. Li, Y. Kang, J.-S. Lu, I. Wyman, S.-B. Ko, S. Wang, *Organometallics* **2014**, 33, 964–973.
- [19] a) C. Lambert, E. Schmäzlin, K. Meerholz, C. Bräuchle, *Chem. Eur. J.* **1998**, 4, 512–521; b) S. Easwaramoorthi, J.-Y. Shin, S. Cho, P. Kim, Y. Inokuma, E. Tsurumaki, A. Osuka, D. Kim, *Chem. Eur. J.* **2009**, 15, 12005–12017; c) S. Easwaramoorthi, P. Thamaraiselvi, K. Duraimurugan, A. J. Beneto, A. Siva, B. U. Nair, *Chem. Commun.* **2014**, 50, 6902–6905; d) B. Dereka, A. Rosspeintner, Z. Li, R. Liska, E. Vauthey, *J. Am. Chem. Soc.* **2016**, 138, 4643–4649.

Manuscript received: November 17, 2021

Accepted manuscript online: February 11, 2022

Version of record online: February 24, 2022